Spring 5-9-2010

The Impact of Thermal Coupling on Catalyst Behavior in Wall-Coated Heat-Exchanger Microreactors

Gregory S. Honda
University of Connecticut - Storrs, gregory.honda@gmail.com

The Impact of Thermal Coupling on Catalyst Behavior in Wall-Coated Heat-Exchanger Microreactors

By

Gregory S. Honda

Submitted to the University of Connecticut in partial fulfillment of the

University Scholars Program,

At the Chemical, Materials, and Biomolecular Engineering Dept.

Author_____

Gregory S. Honda
Dept.: CMBE
Date:

Certified by_____

Benjamin A. Wilhite
Asst. Professor of Chem. Eng.
Thesis Supervisor, Committee Chair

Certified by_____

Ranjan Srivastava
Assoc. Professor of Chem. Eng.

Certified by_____

William Mustain
Asst. Professor of Chem. Eng.

Accepted by_____

Director of University Scholars Prog.

ABSTRACT

Heat exchanger microreactors may be used to couple an exothermic reaction channel to provide the heat necessary for an endothermic reaction in a parallel channel. When wall coated catalysts are employed, the catalytic layers in both channels become an integral part of the heat transfer media. This thesis presents a numerical analysis of the effect on catalyst behavior of thermal coupling for two cases. In the first, a single catalyst layer is modeled under internally heated and internally cooled conditions assuming a constant thermal gradient and neglecting reacting heat. In the second study, both catalyst layers are modeled simultaneously to directly examine the interactions between the exothermic and endothermic catalytic layers. Both studies indicate that thicker catalyst layers are favorable for the exothermic reaction as this allows for the accumulation of heat within the system. Both studies also show that relatively thin catalysts are better for the endothermic reaction and the overall system as this prevents removal of heat while allowing for fast diffusion of the reactant to the hot wall-catalyst interface. The significant interactions between both catalyst layers show the need to develop analytical methods to better understand the intrinsic behavior of the heat-exchanger microreactor system.

Acknowledgements

The author is indebted to Professor B.A. Wilhite for his continued academic and personal support and guidance on this project and throughout the past four years of the author's undergraduate career.

The author also wishes to thank the Honors Program and the University Scholars Program at the University of Connecticut for affording him the opportunity to undertake research as an undergraduate.

The author gratefully acknowledge the financial support of a DuPont Young Professor Grant (FY 2007) and an Office of Naval Research Young Investigator Program Award (#N000140710828) as well as additional financial support from the University of Connecticut Office of Undergraduate Research through a 2009 Summer Undergraduate Research Fund (SURF) award.

TABLE OF CONTENTS

LIST OF FIGURES

Page

I: INTRODUCTION

1.1. Chemical Engineering and Reaction and Diffusion Studies

The primary goal of the chemical engineer is to apply mathematic and analytical techniques to appropriately design working chemical systems. To this end, a variety of specialized fields exist, all of which utilize, to one preferential degree or another, the fundamentals of thermodynamics, kinetics, fluid dynamics, and mass and heat transfer operations. A particularly interesting synergy of these fundamentals occurs within the field of reaction engineering.

Reactors are oftentimes the smallest part of a chemical plant by mass. However, as they are generally the crux of a facility's operations, reactor performance determines the sizing of an entire plant's operations. Appropriate reactor design is thereby crucial in reducing the capital and operating cost of separation trains and other equipment within the plant. Textbook examples of basic reaction engineering include the mathematics behind the design of continuously stirred tank reactors and plug flow reactors [1] for several qualifying scenarios. In both of these cases reactions are assumed to occur on volumetric basis and, in undergraduate courses, are assumed to occur in a homogeneous phase. However, a significant portion of valuable reactions occur heterogeneously between a fluid phase and a solid catalyst.

While it is important to understand the surface science of catalytic reactions in order to develop a catalyst with a favorable reaction mechanism, one also needs to consider the performance of the catalyst when physically introduced to a real reactor. As most catalysts are composed of precious and rare-earth metals, they are typically mixed in low mass percentages with alumina or other comparable metal oxides. This dispersion forms a solid network of pores

of varying dimensions within individual catalyst particles. Within a reactor, the porous catalytic particle is typically introduced as either a collection of catalytic pellets of uniform dimensions (as in a packed bed reactor), as a catalyst powder, a thin film along the reactor walls, or is directly incorporated within a fabricated support. In any case, reacting species must diffuse through the porous networks of a catalytic particle of characteristic dimensions in order to react with active catalyst sites. One would therefore surmise that diffusion limitations ought to restrict the reaction to the outer layers of a catalyst grain. The competition between rates of diffusion and reaction of chemical species would then result in the compromise of reactor performance. To this end enters the study of reaction and diffusion.

1.2. Ernest W. Thiele and the Fundamentals of Reaction and Diffusion

The theory that the interior compositions of reacting specie are non-uniform within a catalyst and would consequentially impact catalyst performance was first proven analytically by E.W. Thiele in 1939 in his paper "Relation between Catalytic Activity and Size of Particle" as published in *Industrial and Engineering Chemistry* [2]. To investigate the aforementioned phenomena, the ratio of actual reaction rate to the reaction rate in the absence of any transport limitations was determined. This value, referred to as the catalyst effectiveness, was calculated for several base case scenarios: the first and second order reaction where the catalyst is in flat plates, the first order reaction in a spherical pellet, and several cases for the first order reaction in a flat plate where reaction is accompanied by a change in a volume.

The assumptions inherent within his study, and which build the basis for all subsequent reaction and diffusion studies, are as follows. The reacting fluid is of a single phase though it can be either a liquid or gas. The fluid surrounding the catalytic particle is assumed to be of a

constant and spatially uniform composition. Diffusion from the bulk fluid through any surface film surrounding the particle is assumed to be rapid relative to the rates of interior diffusion within the particle. Reaction heat is not considered and the temperature within the catalyst is assumed to be uniform and constant. Also, the reaction is assumed to take place along the walls of the largest catalyst pores while reaction at the actual external surface of the particle is assumed to be negligible. Furthermore, the rate is specified based on the area of the largest pore, though the actual reaction may occur in subsequently smaller pore structures. The cross sectional area of the specified pore is also assumed to be constant and representative of an average. Finally, the reverse reaction is assumed to be negligible and convective mass transfer is assumed to not occur.

In order to elucidate the analytical solution determined by Thiele, the derivation of the analytical solution for diffusion and reaction subject to the previous assumptions is presented below for the case of a single, nth order reaction occurring within a flat plate.

$$Input = -D_{eff} \cdot A \cdot \left.\frac{dC_A}{dx}\right|_x \quad \text{and} \quad Output = -D_{eff} \cdot A \cdot \left.\frac{dC_A}{dx}\right|_{x+\Delta x} + k \cdot (A\Delta x) \cdot C_A^n \qquad (1.1)$$

Assuming steady state: *Input* = *Output*

and taking the limit as $\Delta x \rightarrow 0$ with constant effective diffusivity, D_{eff}, then:

$$D_{eff} \cdot \frac{d^2 C_A}{dx^2} = k_f C_A^n \qquad (1.2)$$

Which, when rendered dimensionless yields:

$$\frac{d^2 u_A}{ds^2} = \phi_A^2 u_A^n \qquad (1.3)$$

Where $u_A = \frac{C_A}{C_{Af}}$, $s = \frac{x}{L}$ and $\phi_A^2 = \frac{k_f L^2 \cdot C_{Af}^{n-1}}{D_{eff}}$ where ϕ_A is the Thiele modulus for species A.

Considering the boundary conditions such that no flux occurs at the wall interface and that the concentration at the fluid-solid interface is equivalent to the bulk fluid concentration (*Dirichlet* condition):

$$\frac{du}{ds} = 0 \quad \text{at} \quad s = 0 \tag{1.4a}$$

and $u = 1$ at $s = 1$ (1.4b)

In order to gain insight into impact of diffusion limitations on reaction rate, the effectiveness factor, η, is defined as the ratio of the rate of reaction to the reaction rate in the absence of all transport limitations.

$$\eta = \frac{\int_0^L kC_A^n (Adx)}{\int_0^L kC_{Af}^n (Adx)} \quad \rightarrow \quad \eta = \int_0^1 u_A^n \cdot ds \tag{1.5a}$$

Substituting in eq. 1 for u_A:

$$\eta = \frac{1}{\phi_A^2} \int_0^1 \frac{d^2 u_A}{ds^2} \cdot ds \quad \rightarrow \quad \eta_h = \frac{1}{\phi_h^2} \cdot \frac{du_h}{ds}\bigg|_0^1 \tag{1.5b}$$

Given the simplicity of this single, isothermal reaction, an appropriate analytical solution may be determined. The general solution is:

$$u(s) = c_1 \cosh(\phi s) + c_2 \sinh(\phi s) \tag{1.6a}$$

$$\frac{du}{ds} = \phi[c_1 \sinh(\phi s) + c_2 \cosh(\phi s)] \tag{1.6b}$$

Substitution of the boundary conditions (Eqn. 1.4) yields:

$$c_2 = 0$$

$$c_1 = \frac{1}{\cosh(\phi)}$$

Therefore, the solution to () is given by:

$$u(s) = \frac{\cosh(\phi s)}{\cosh(\phi)} \tag{1.7a}$$

and the effectiveness for an isothermal slab is:

$$\eta = \frac{\tanh(\phi)}{\phi} \tag{1.7b}$$

The resulting dependencies of effectiveness on the Thiele modulus as determined by Thiele are presented in Figure 1.1.

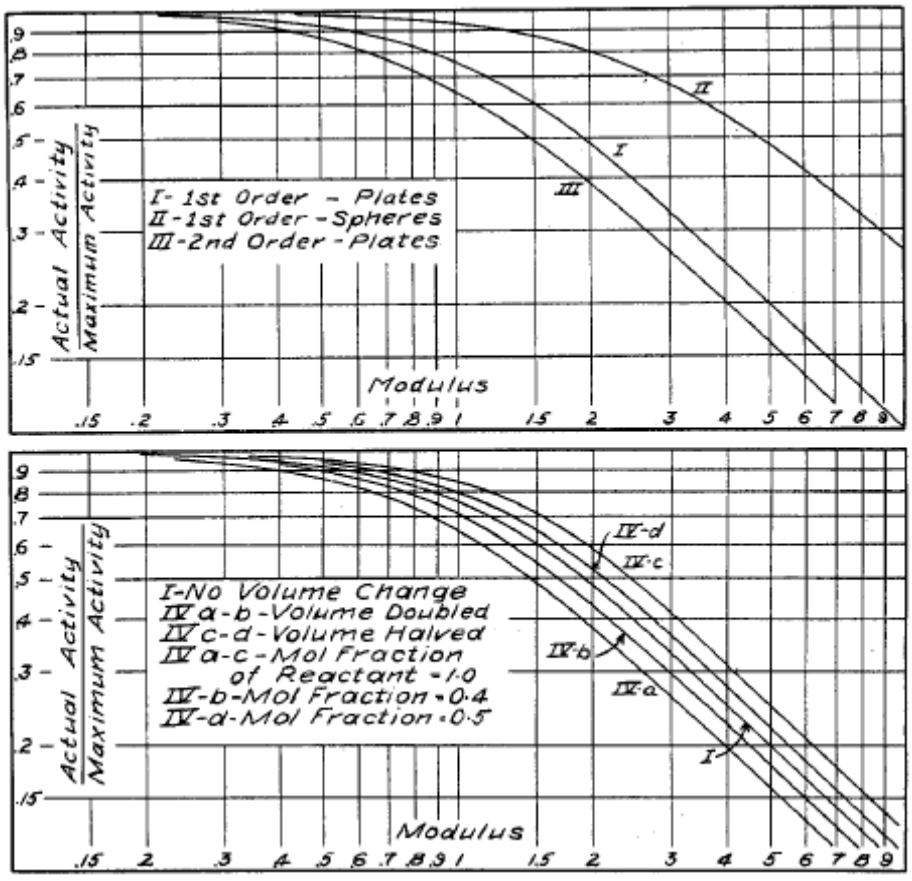

Figure 2.1: Results by Thiele of the effectiveness versus the Thiele modulus.

The observable trends between all cases are similar, showing values of effectiveness near one for values of the Thiele modulus sufficiently less than unity. Thiele interpreted these results as indicating that a below a specific grain size (low value of ϕ or low diffusion limitation relative to particle size) the associated value of unity for the effectiveness suggests that the catalyst volume will control the reaction rate (essentially rate limited). For values of ϕ greater than this value, the catalyst external surface will determine reaction rate (diffusion limited).

1.3. Reaction and Diffusion Analysis, 1937-Present

Since the paper by Thiele, the interplay of diffusion and chemical reaction within catalytic elements exposed to uniform external concentration and temperature has been thoroughly investigated for more complicated scenarios of isothermal reactions in particles of non-uniform geometry [3] and reactions with complex kinetics [4, 5], as well as non-isothermal situations where reaction heat may accumulate within the catalyst [5, 6]. For the case of an individual pellet length scale that is substantially smaller than the relevant reactor scale, the assumption of uniform external (or bulk fluid) conditions bounding the catalytic element remains valid [1]; this in turn enables insight into catalyst performance *independent of reactor-scale considerations*. However, concentration and thermal gradients become substantial when reactor length scales are equivalent to those of the catalyst element [7], or when the catalyst is directly involved in heat [8, 9, 10] and/or mass transfer [11, 12] between separate fluid volumes. Under such circumstances bulk-fluid concentration and thermal gradients, which are typically observable only at the reactor scale, result in exposure of catalytic elements to non-uniform conditions. These cases require consideration of externally imposed gradients upon the catalytic region.

Aris and Copelowitz [7] considered the case of exothermic reaction in a jacketed, catalytic packed-bed reactor in which limited fluid-phase heat transfer rates result in substantial radial thermal and concentration gradients across the packed bed. If the resulting radial gradients are of sufficient magnitude, individual catalytic elements may be exposed to non-uniform external boundary conditions. Aris & Copelowitz therefore studied a spherical catalyst element subjected to external temperature and concentration that varied linearly along the surface of the sphere with respect to the polar axis of the particle. The resulting model provided insight into the influence of externally applied gradients to a symmetrical catalyst element, in particular showing the stabilizing impact of external gradients by reduction in the range of Thiele modulus for which multiplicity can occur. While this case considered system temperature and concentration gradients as an unintentional (and undesirable) consequence to be accounted for, purposefully forced external gradients may also be a critical design aspect of the reaction system.

1.4. Motivation and Summary of Thesis

Such an instance is exemplified by catalytic-wall heat-exchanger reactors, in which an exothermic reaction acts as the heat source for an endothermic reaction occurring in a separate channel [13, 14]. This juxtaposition gives rise to steep thermal gradients across the media separating the channels, with the magnitude of the resulting thermal gradient being dependent upon both materials selection and system design. By affecting heat-exchanger reactor designs in microchannel networks (i.e., microreactors), substantial reduction in fluid-phase heat and mass transfer limitations may be achieved due to reduced hydraulic diameters, while enhanced rates of fluid-solid heat transfer are achieved owing to increased surface area-to-volume ratios [15, 16]. However, to avoid excessive pressure drops associated with packed catalyst beds, the catalyst

phase is often introduced as a diffusive film on the channel surface via slurry coating [17, 18]. In this configuration, heat transfer between individual fluids occurs through both the inert supporting walls as well as the catalyst phase; the relatively low thermal conductivity of a ceramic-based porous catalytic washcoating, compared to the thermal conductivity of stainless steels or silicon which typically comprise the microchannel network, can be expected to focus this externally forced thermal gradient within the catalytic phase. Thus, the diffusive catalytic volume is subjected to an externally imposed thermal gradient, becoming an integral component of the heat transfer media. While numerous analyses of heat-exchanger microreactor configurations and flow patterns have been performed [19, 20, 21, 22, 23], these investigations have considered the reactor system as a whole.

This thesis provides two approaches to gaining insight into the behavior of coupling exothermic and endothermic channels in a heat-exchanger microreactor. In the first, a single catalyst layer is modeled in the presence of a constant thermal gradient and the absence of reaction heat. This allows for consideration of the effect of significant differences between the bulk fluid temperatures of the coupled channels. In the second study, heats of reaction are taken into account and the endothermic and exothermic catalyst layers are modeled simultaneously. This provides direct insight into the interactions and interdependencies between the coupled catalyst layers.

II: THE CONSTANT THERMAL GRADIENT CASE

2.1. Model Derivation

In the present study, the authors consider the reaction and diffusion of arbitrary chemical species *A* through a catalytic film bounded by an impermeable, non-reactive wall at fixed temperature T_w and a fluid of constant concentration C_{Af} and fixed temperature T_f (Figure 2.1). This approximates the catalyst film as it occurs in a heat-exchanger reactor configuration, only such that the catalytic film model is isolated from the larger heat-exchanger system model. Derivations of the model equations for this system with (i) a single reaction and two reactions competing in (ii) parallel and (iii) series are presented below.

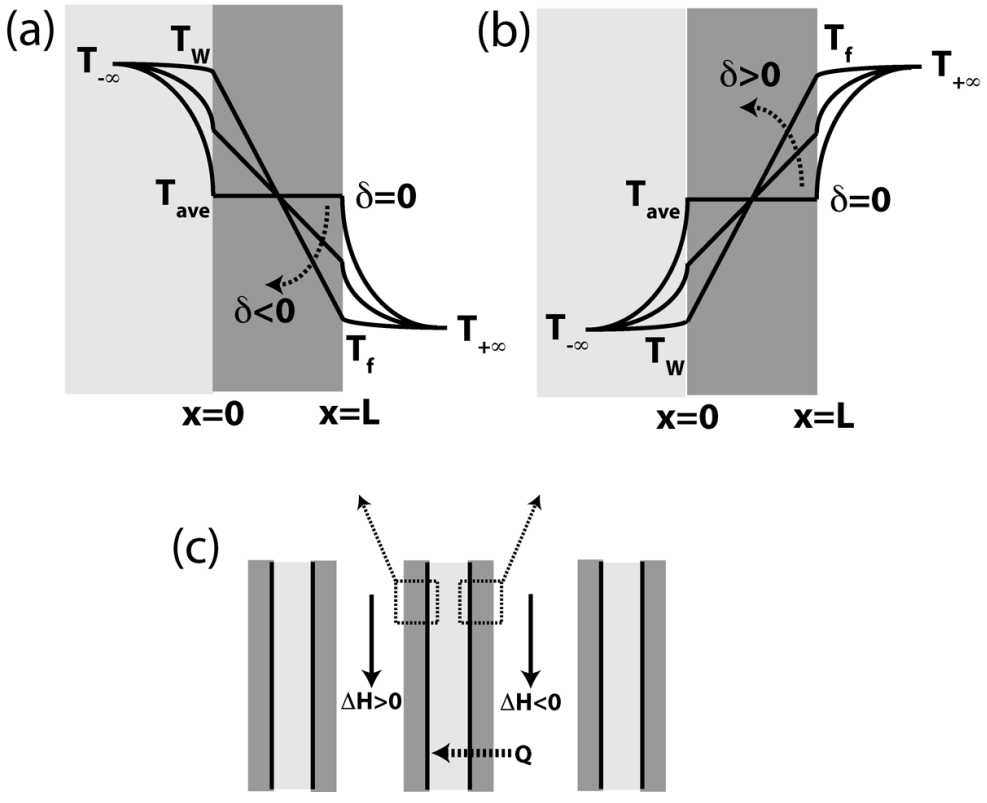

Figure 2.1: Steep thermal gradients arising from coupling of endothermic and exothermic channels.

2.1.1. Case I: Single Irreversible Reaction, $A \xrightarrow{n} B$

A single, irreversible & elementary mole-neutral reaction of the form $A \xrightarrow{n} B$ is assumed to occur in tandem with diffusive mass transport within the catalyst volume. The catalyst washcoating is approximated as a Cartesian slab of thickness L. Thus, the steady-state mass balance of species *A* is described by the second-order differential equation:

$$D_{Aeff} \cdot \frac{d^2 C_A}{dx^2} = k_n C_A^n \tag{2.1}$$

For the present analysis, constant wall and fluid temperatures are assumed, while simultaneously neglecting reaction heat generated within the diffusive volume. This in turn isolates the consideration of reaction and diffusion within a single catalytic film from the more complex macroscopic model of the heat-exchanger reactor system, in a fashion analogous to the classical treatment of reaction and diffusion in an individual catalyst element [24]. By assuming constant temperature boundary conditions and neglecting reaction heat within the diffusive volume, a linear steady-state thermal gradient is imposed upon the reaction-diffusion problem, as follows:

$$T = \left[\left(T_f - T_w \right) \left(\frac{x}{L} - 1 \right) \right] + T_f \tag{2.2}$$

Rendering Equations (2.1) and (2.2) dimensionless in terms of the bulk fluid concentration and temperature and combining, a single governing differential equation may be obtained:

$$\frac{d^2 u_A}{ds^2} = \phi_f^2 \cdot \exp\left[\gamma_n \cdot \left\{ \frac{\delta(s-1)}{1+\delta(s-1)} \right\} \right] \cdot u_A^n, \tag{2.3}$$

where $u_A = \frac{C_A}{C_{Af}}$, $s = \frac{x}{L}$, $\gamma_n = \frac{E_n}{RT_f}$, $\delta = \frac{T_f - T_w}{T_f}$, and $\phi^2 = \frac{k_{nf} L^2 C_{Af}^{n-1}}{D_{Aeff}}$. The latter governing dimensionless parameter is the Thiele modulus relative to the *observable* fluid temperature, such that $k_{nf} = k_0 \exp\left(\frac{-E_n}{RT_f}\right)$. Employing the bulk fluid temperature as the reference temperature for this system allows direct analysis of the influence of internal heating or cooling of the catalyst with respect to the observable fluid temperature, as well as providing catalyst effectiveness and selectivity models that may be easily combined with macroscale mixing models governing the bulk fluid properties. This methodology additionally allows the models to retain their "classical" form with respect to γ and ϕ, similar to previous studies of non-isothermal reaction and diffusion in catalysts [6, 7, 24].

Assuming no external fluid-solid transport limitations and recognizing an impermeable reactor wall, *Dirichlet* boundary conditions at the external fluid-solid interface and zero-flux conditions at the internal catalyst-wall interface are applied, i.e.:

$$u_A = 1 \quad \text{at} \quad s = 1 \tag{2.3a}$$

and

$$\frac{du_A}{ds} = 0 \quad \text{at} \quad s = 0 \tag{2.3b}$$

This non-linear second order differential equation can be solved numerically to obtain the dimensionless concentration profile within the catalyst region. An effectiveness factor, η, may be defined as the ratio of the actual rate of reaction in the presence of the forced thermal gradient to the rate of reaction if the catalyst zone were operated at a uniform temperature equal to the average of T_w and T_f in the absence of mass transport limitations. The latter case represents an ideal scenario corresponding to rapid heat and mass transfer across the catalyst layer such that the temperature within the catalyst is constant while retaining a quantity of thermal energy in the

solid phase identical to that for the corresponding thermal gradient case. These two cases thus shape the implicit assumption that fluid-phase and wall-phase heat transfer limitations are equal.

$$\eta = \frac{\int_0^L k_n(T) \cdot C_A^n \cdot A dx}{\int_0^L k_n(T_{Avg}) \cdot C_{Af}^n \cdot A dx} \tag{2.4a}$$

$$\text{Where: } T_{avg} = T_f\left(1 - \frac{\delta}{2}\right) \tag{2.4b}$$

Rendering dimensionless and substituting definitions for T_{ave} and k_n results in the following definition for effectiveness:

$$\eta = \exp\left[\alpha_n \cdot \left\{\frac{\delta}{2-\delta}\right\}\right] \cdot \int_0^1 u_A^n \exp\left[\gamma_n \cdot \left\{\frac{\delta(s-1)}{\delta(s-1)+1}\right\}\right] \cdot ds \tag{2.4c}$$

Substituting the integrand for the second derivative of Eqn. 2.3 yields the final definition of effectiveness.

$$\eta = \frac{1}{\phi^2} \exp\left[\gamma_n \cdot \left\{\frac{\delta}{2-\delta}\right\}\right] \cdot \left.\frac{du_A}{ds}\right|_0^1 \tag{2.4}$$

The resulting model for a single irreversible reaction offers significant insight into catalyst effectiveness under externally applied thermal gradients. Models are also developed to investigate the influence of thermal gradients upon series and parallel selective reaction networks, as detailed below.

2.1.2. Case II: Two Consecutive Reactions, $A \xrightarrow{n} B \xrightarrow{m} C$

The same assumptions, boundary conditions, and equations as developed for species *A* in the single reaction hold for the series reaction. In addition, the mass balance for species B can be written:

$$D_B \cdot \frac{d^2 C_B}{dx^2} = k_m C_B^m - k_n C_A^n \tag{2.5}$$

which when rendered dimensionless and substituting the thermal gradient function becomes:

$$\frac{d^2 u_B}{ds^2} = \phi^2 \cdot D_{A/B} \cdot \exp\left(\gamma_n \left\{ \frac{\delta(s-1)}{\delta(s-1)+1} \right\} \right) \times$$

$$\left(u_B^m \kappa_{mnf} \exp\left[\gamma_n \cdot (\varepsilon_{mn} - 1) \cdot \left\{ \frac{\delta(s-1)}{\delta(s-1)+1} \right\} \right] - u_A^n \right) \tag{2.6}$$

where $\kappa_{mnf} = \frac{C_{Af}^m}{C_{Af}^n} \cdot \frac{k_{mf}}{k_{nf}}$, $D_{A/B} = \frac{D_A}{D_B}$ and $\varepsilon_{mn} = \frac{\gamma_m}{\gamma_n}$. Assuming there is no amount of species *B* in the bulk fluid, the boundary conditions for species *B* are:

$$u_B = 0 \quad \text{at} \quad s = 1 \tag{2.6a}$$

and $$\frac{du_B}{ds} = 0 \quad \text{at} \quad s = 0 \tag{2.6b}$$

For the non-trivial case of intermediate reaction species B being the desired product, it is appropriate to define selectivity of the entire catalyst film as follows:

$$S = \frac{r_B}{r_B + r_C} = -\frac{r_B}{r_A} = \frac{\int_0^1 -\frac{1}{\phi^2} \frac{1}{D_{A/B}} \frac{d^2 u_B}{ds^2} \cdot ds}{\int_0^1 \frac{1}{\phi^2} \frac{d^2 u_A}{ds^2} \cdot ds} = -\frac{1}{D_{A/B}} \cdot \frac{\left. \frac{du_B}{ds} \right|_0^1}{\left. \frac{du_A}{ds} \right|_0^1} \tag{2.7a}$$

The conditions which favor the desired product differ significantly between series and parallel reactions in conventional reactors. As such, equations describing the parallel reactions are developed below to further investigate the impact of a forced thermal gradient on selectivity.

2.1.3. Case III: Parallel Reactions, $A \xrightarrow{n} B$, $A \xrightarrow{p} D$

Similar treatments as those developed for the single and series reactions can be applied to the parallel reactions. Retaining the previously stated assumptions and boundary conditions, the mass balance for species *A* yields the following differential equation:

$$\frac{d^2 u_A}{ds^2} = \phi^2 \cdot \exp\left(\gamma_n \left\{ \frac{\delta(s-1)}{\delta(s-1)+1} \right\} \right) \times$$

$$\left(u_A^n + u_A^p \kappa_{pnf} \exp\left[\gamma_n \cdot (\varepsilon_{pn} - 1) \cdot \left\{ \frac{\delta(s-1)}{\delta(s-1)+1} \right\} \right] \right) \tag{2.8}$$

where $\kappa_{pnf} = \frac{C_{Af}^p}{C_{Af}^n} \cdot \frac{k_{pf}}{k_{nf}}$ and $\varepsilon_{pn} = \frac{\alpha_p}{\alpha_n}$. The dimensionless mass balance for species *B* can be written as:

$$\frac{d^2 u_B}{ds^2} = \phi_f^2 \cdot D_{A/B} \cdot \exp\left(\gamma_n \left\{ \frac{\delta(s-1)}{\delta(s-1)+1} \right\} \right) \cdot \left(-u_A^n \right) \tag{2.9}$$

Selectivity of species *B* can again be determined by analysis of rates:

$$S = \frac{r_B}{r_B + r_D} = -\frac{r_B}{r_A} = -\frac{1}{D_{A/B}} \cdot \frac{\left. \frac{du_B}{ds} \right|_0^1}{\left. \frac{du_A}{ds} \right|_0^1} \tag{2.7b}$$

Which is equivalent to the expression developed for the series reaction. The resulting system of ordinary differential equations is analyzed to determine the influence of Thiele moduli, reaction activation energies and thermal gradient magnitude upon catalyst performance.

2.2. Procedure

The above boundary value problems were solved numerically using Matlab (v7.7.0) software for the single, series, and parallel reaction cases. In all cases the software package *bvp4c*, employing Simpson's method, was used to obtain solutions. The derivatives of the species were used to determine effectiveness factors and selectivities for a range of parameter values.

2.3. Results and Discussion

2.3.1. Case I: Single Reaction

The calculated values of the effectiveness factor as a function of γ, δ, and ϕ for the single, first-order reaction are presented in Figure 2.2. It is worth noting that the solution for $\delta = 0$ corresponds to the classic solution of isothermal reaction with internal diffusion limitations [1]. In all cases of $\delta \neq 0$, there exists within the catalyst film a high-temperature and a low-temperature zone (relative to the average temperature for $\delta = 0$) of equal volume. In the absence of diffusion limitations, the hot region is capable of outpacing the low-temperature zone substantially owing to the non-linear Arrhenius relation of reaction rate with temperature.

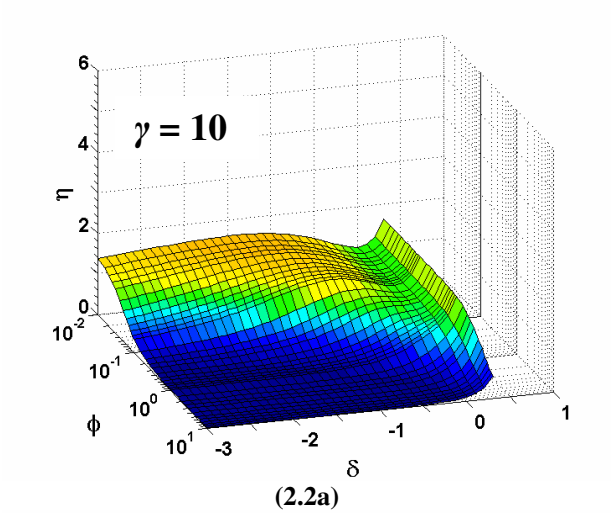

(2.2a)

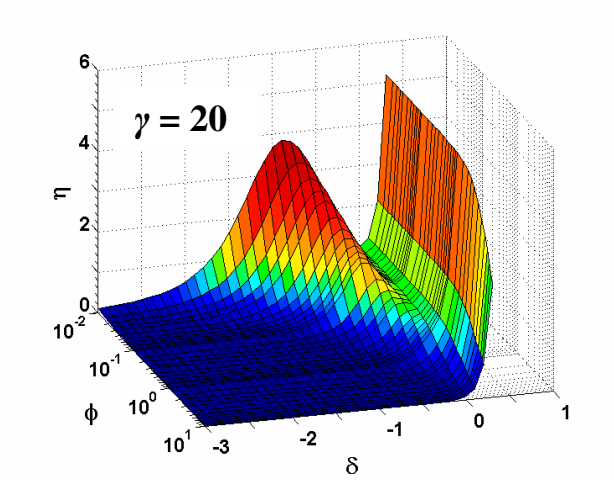

(2.2b)

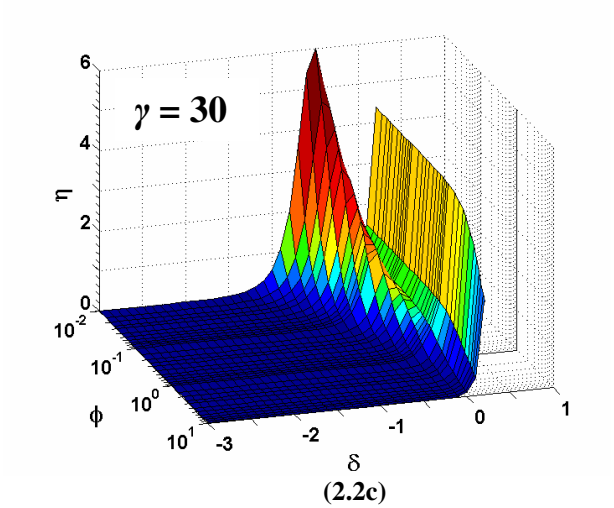

(2.2c)

Figure 2.2: Effectiveness plots for the single reaction for three values of γ.

For the case of $\delta > 0$ (corresponding to $T_f > T_w$, or an internally cooled catalyst layer), the effectiveness increases rapidly with δ regardless of Thiele moduli. This is due to the placement of the high-temperature zone adjacent to the reactant zone, i.e. the fluid phase, such that diffusional limitations are minimized. For the case of $\delta < 0$ ($T_f < T_w$ or internally heated), mild enhancement in catalyst efficiency is possible only at low values of the Thiele moduli; otherwise substantial losses in effectiveness are predicted due to diffusional limitations which restrict reaction to the low-temperature zone, now placed adjacent to the fluid. Figure 2.2 presents three surface maps of the two-dimensional $\delta - \phi$ parameter space for increasing values of activation energy (γ); it is seen that as α increases, the magnitude of enhancement increases, while the general shape of the effectiveness surface remains the same.

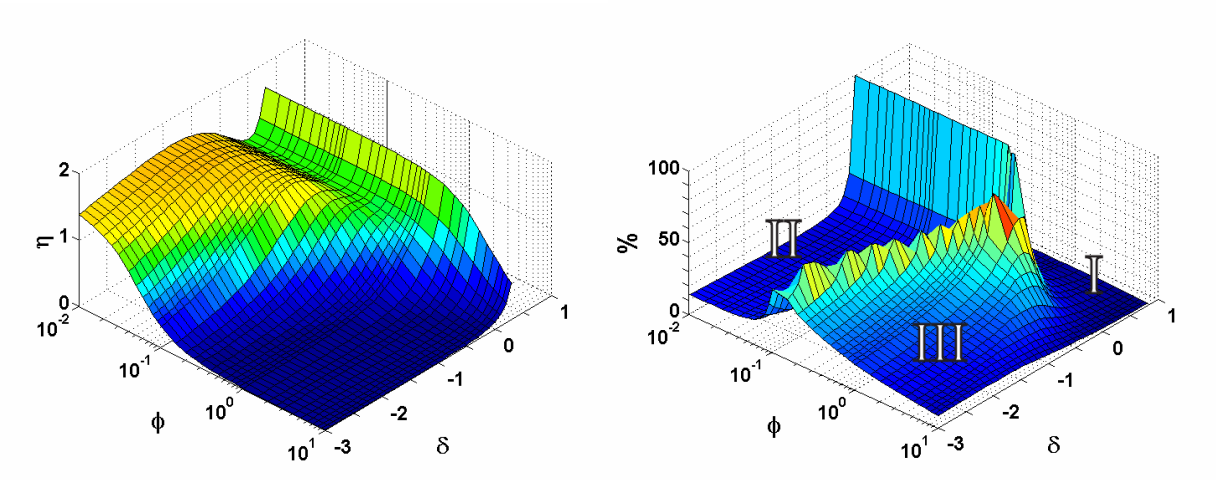

(2.3a) **(2.3b)**

Figure 2.3: Close up of the effectiveness (2.3a) and catalyst utilization (2.3b) for γ = 10.

Figure 3a presents a close-up of the region of catalyst enhancement for the case of an internally heated catalyst ($\delta < 0$) at $\gamma = 10$. This region of catalyst enhancement is bounded by the $\delta = 0$ case (isothermal) and a vector spanning decreasing ϕ with decreasing δ. Additional insight into the origin of this vector may be obtained by studying the percentage of catalyst that

contributes substantially to the reaction, which is not explicitly accounted for by the effectiveness factor. For example, high effectiveness is observed at $\delta > 0$ and $\phi >> 1$ due to a small, high temperature region operating at rapid reaction rates even while the majority of the catalyst contributes negligible conversion, i.e. goes unused. Figure 2.3b presents the percentage of total catalyst volume operating at > 75% of the maximum reaction rate, as determined from each corresponding concentration and temperature profile. The trends observed in effectiveness can be seen to be complemented by trends with respect to catalyst utilization. For $\delta = 0$, virtually all of the catalyst operates at or near the maximum rate when $\phi < 1$. This narrow region of high catalyst utilization appears to bound the $\eta > 1$ region of the ϕ versus δ phase space at $\delta < 0$ (shown in Figure 2.3a); in conjuction with the $\delta = 0$ (isothermal) case, the ϕ versus δ phase space can thus be separated into three distinct regions as indicated in Figure 2.3b. A sampling of concentration profiles for five values of ϕ and δ, corresponding to each region and points traversing the high catalyst utilization vector are presented in Figure 2.4.

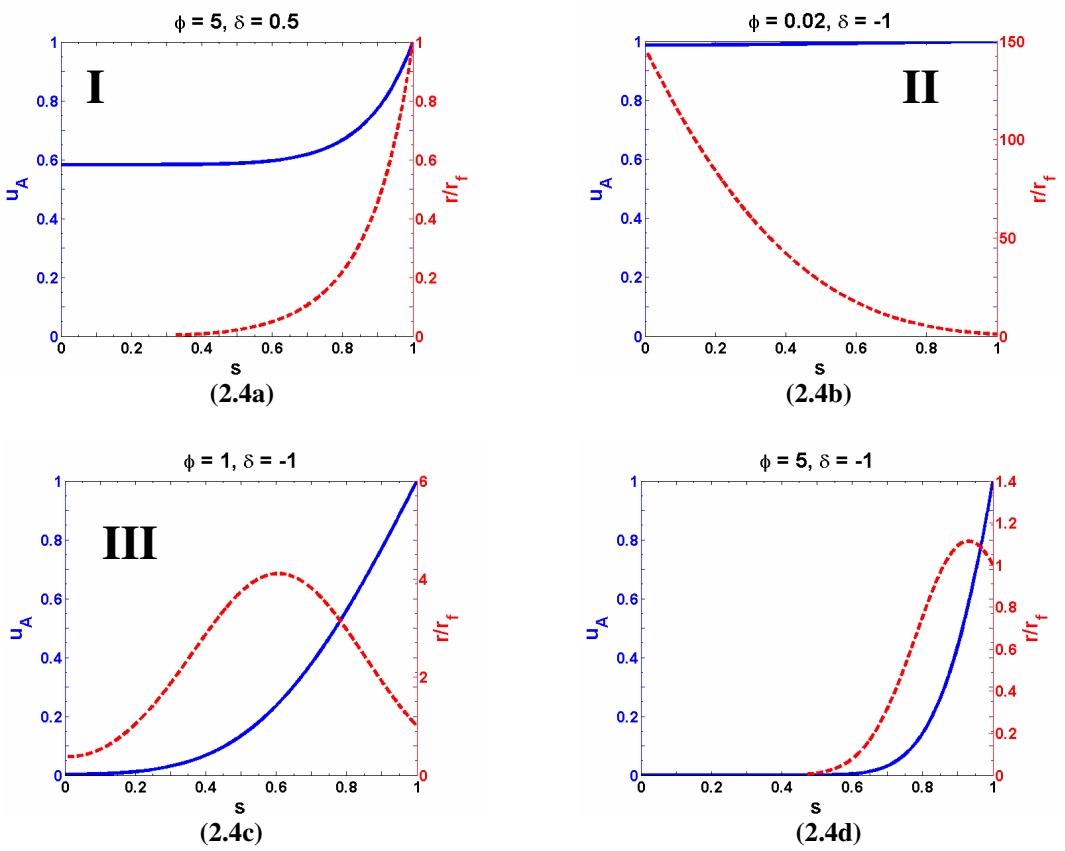

Figure 2.4: Internal profiles of dimensionless concentration and relative reaction rate {γ = 10}.

Region I, occurring at $\delta > 0$, corresponds to the majority of reaction taking place in a region near the fluid-catalyst interface, owing to the elevated catalyst temperature therein. Region II, occurring at $\delta < 0$ and low values of ϕ, corresponds to the case of the majority of reaction taking place in a region near the wall-catalyst interface as a result of the elevated temperature of the catalyst and the absence of mass transfer limitations. In Region III, this high temperature region is depleted of reactants due to accumulated diffusion limitations; with a maximum in local reaction rate occurring at a finite depth from the fluid-catalyst interface as controlled by the diffusional penetration of the reactant. This influence of the Thiele moduli upon dictating a highly active region with the catalyst layer is illustrated by Figure 2.4c.

2.3.2. Case II: Two Consecutive Reactions

Selectivity analysis for the case of two consecutive reactions was performed for $\gamma = 20$, n = m = 1 and $\kappa_{mnf} = 2$ at four values of ε_{mn} to investigate the influence of δ upon selectivity as the ratio of undesired to desired reaction activation energy increases. It is important to recognize that the determined selectivity represents the additional selectivity contributed by diffusion limitations and thermal effects within the catalyst, and not the intrinsic selectivity of a particular catalyst for the reaction network. As defined, the selectivity of the consecutive-reaction network is equivalent to unity where these additional effects have no impact upon overall selectivity. Resulting surface maps are presented in Figure 2.5, noting that all four surfaces share the identical $S(\phi)$ curve at $\delta = 0$, corresponding to the reference case of an isothermal catalyst slab.

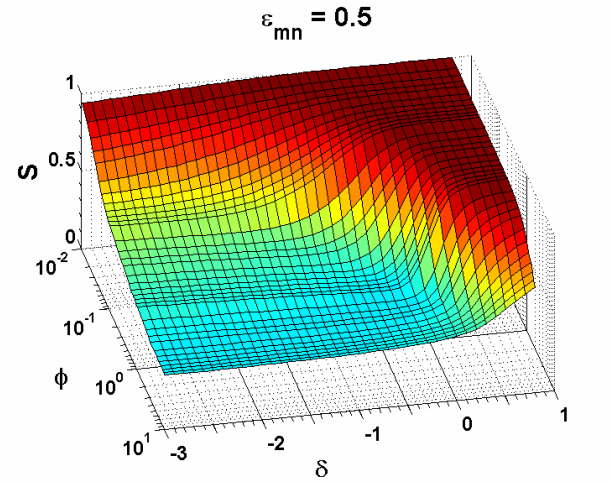

(2.5a)

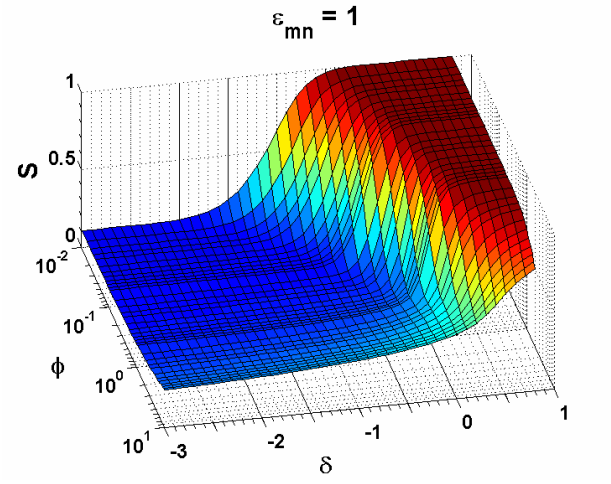

(2.5b)

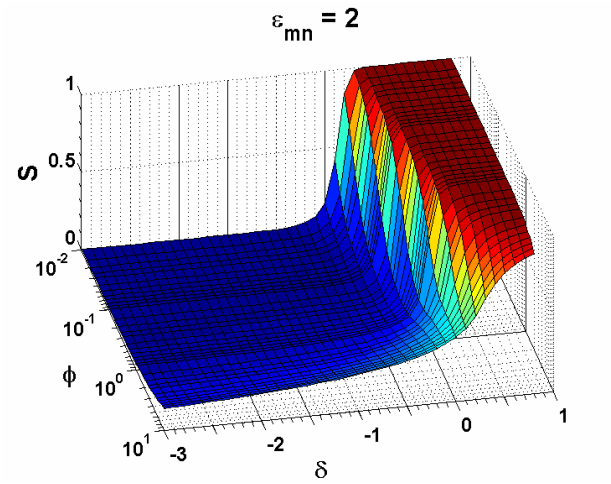

(2.5c)

Figure 2.5: Selectivity for consecutive series reactions {γ = 20, n=m=1, κ_{mnf} = 2}.

Recall that for the isothermal case ($\delta = 0$) at $\phi \leq 0.1$ the concentrations throughout the catalyst layer reflect the conditions at the fluid-catalyst interface, which for the present case is $u_A = 1$, $u_B = 0$. This in turn implies that the rate of the second reaction is negligible as diffusion is able to remove any desired product from the catalyst before it can be further reacted. Thus, a unity selectivity (100%) is predicted at low values of ϕ. As ϕ increases, the desired product B accumulates within the catalyst, allowing the undesired reaction to occur and resulting in a drop in selectivity.

For the case of $\delta > 0$, selectivity is observed to increase with δ for a given ϕ value; this reflects the fact that the most active catalytic region is now closest to the point of desired product removal (i.e. the fluid-catalyst interface) which in turn allows the diffusive removal of intermediate product B before it can be further reacted. From Figure 2.5, it can be seen that two-fold or greater improvements in selectivity can be achieved by maintaining an externally imposed thermal gradient ($\delta > 0$) at values of $\phi \geq 0.5$. Thus, the use of thicker catalyst layers is expected to result in more pronounced thermal gradients and higher values of ϕ may be expected to maintain high conversion rates and selectivities for the case of an internally-cooled catalyst.

For the case of $\delta < 0$, a further decrease in selectivity is predicted as higher temperatures within the catalyst interior cause both desired and undesired reactions to proceed more rapidly relative to reaction at the fluid-solid interface. After forming in the catalyst interior, the desired product B is therefore more likely to react before diffusing out of the catalyst. As ϕ increases, greater diffusion limitations further prevent removal of the desired product B which causes an additional decrease in selectivity.

The influence of varying the ratio of undesired to desired reaction activation energies (ε_{mn}) upon selectivity is also illustrated in Figure 5. It is important to note that in rendering the system of equations dimensionless, the bulk fluid temperature was selected as the fixed reference point; this in turn means that by varying δ the average temperature of the catalyst is also varied. Specifically, for the case of an internally-cooled catalyst (i.e. $\delta > 0$), the average catalyst temperature is less than that of the $\delta = 0$ reference case. Likewise, for the case of an internally-heated catalyst (i.e. $\delta < 0$), the average catalyst temperature is greater than that of the $\delta = 0$ reference case. Thus, for $\varepsilon_{mn} > 1$ increasing the average catalyst temperature ($\delta < 0$) favors the undesired reaction and decreases selectivity, while decreasing catalyst temperature ($\delta > 0$) increases selectivity. These additional gains in selectivity are muted by diffusional limitations occurring at high ϕ values. In this manner, increasing ε_{mn} effectively reduces the region of high selectivity available for internally-heated catalysts ($\delta < 0$).

However, for values of $\varepsilon_{mn} < 1$, the inverse relationship is not observed. Though selectivity is higher for $\delta < 0$, diffusion limitations at moderate values of ϕ prevent reactants from reaching the wall-side of the catalyst where higher temperatures favor the desired reaction. Furthermore, the selectivity for the desired species B remains high for $\delta > 0$ despite being thermally unfavorable. As previously discussed, this effect is a result of the favorability of the fluid-side position of the active zone within the catalyst layer which allows for rapid removal of the desired product. *As such, the position of the active zone within the catalyst layer is the dominating factor in determining selectivity for the series reaction.*

2.3.3. Parallel Reactions:

Selectivity for the case of two competing (parallel) reactions was analyzed for $\gamma = 20$, n = 2, p = 1, and $\kappa_{pnf} = 1$, such that the desired reaction is of the higher order. Figure 2.6 presents maps of the selectivity over the $\delta - \phi$ parameter space for four different values of ε_{pn}, including cases where the desired reaction is favored by lower temperatures ($\varepsilon_{pn} < 1$) and high temperatures ($\varepsilon_{pn} > 1$). For the isothermal case of $\delta = 0$, the selectivity at low values of ϕ corresponds to a unity dimensionless reactant concentration throughout the catalyst, such that the reaction-diffusion zone favors each reaction equally (i.e. $S = 0.5$). As ϕ increases, the diffusional limitations result in a depleted internal region that favors the lower-order reaction, such that the catalyst introduces additional selectivity towards the undesired reaction. For the case of $\varepsilon_{pn} = 1$ (Figure 2.6b), such that selectivity is invariant with temperature, the above trend combines with that of decreasing selectivity with decreasing δ, where internal heating of the catalyst results in a large percent of the catalyst volume that is depleted, thus favoring the lower-order reaction.

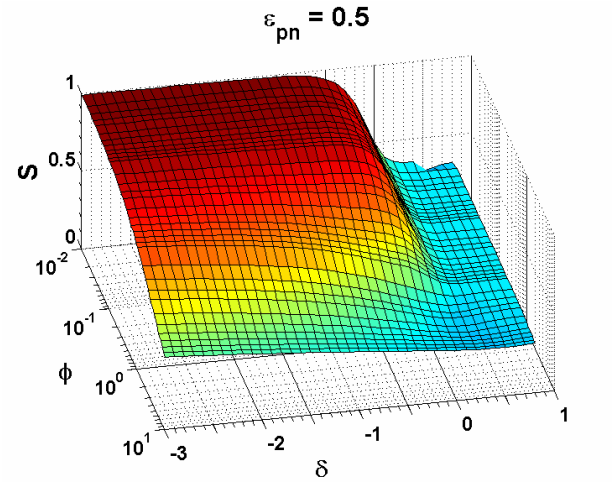

(2.6a)

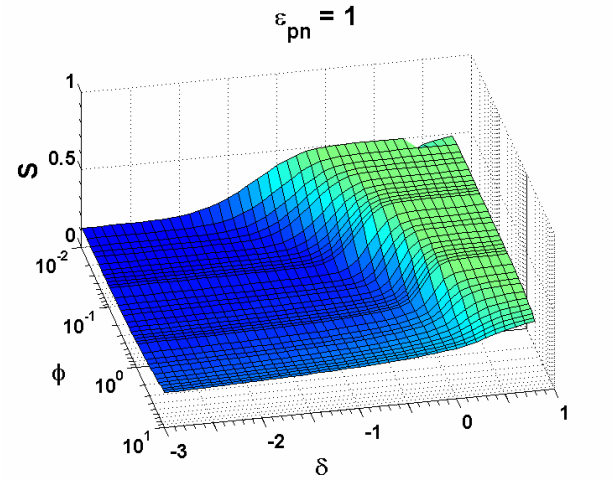

(2.6b)

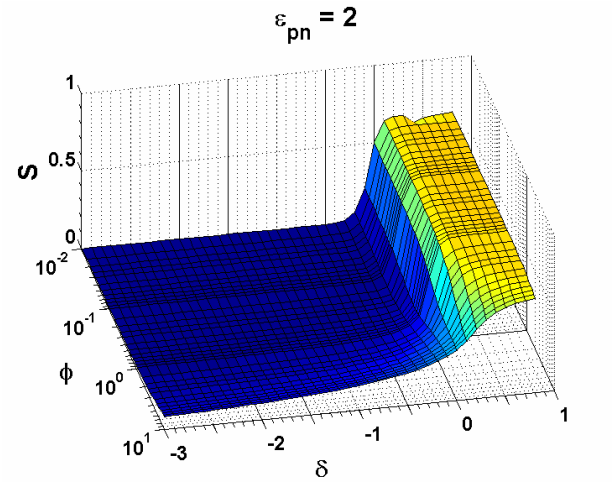

(2.6c)

Figure 2.6: Selectivity for the case of parallel reactions {$\gamma = 20$, $n = 2$, $p = 1$, and $\kappa_{pnf} = 1$}.

For the case of $\varepsilon_{pn} < 1$ (where increasing temperature favors the desired reaction) additional gains in selectivity are observed for $\delta < 0$ (corresponding to an increase in average catalyst temperature); conversely, if $\varepsilon_{pn} > 1$, gains in selectivity are observed at $\delta > 0$ due to additional thermal effects. As such, the selectivity of the parallel reaction is entirely thermally dependent. In both cases, these effects are muted by diffusional limitations at high values of ϕ.

2.4. Conclusions

The modeling of a constant thermal gradient enabled a systematic analysis of the influence of externally-applied thermal gradients upon catalyst performance and utilization, which represents a unique contribution in the consideration of reaction and diffusion in a catalytic volume. This in turn provides valuable insight into the design of catalytic-wall heat-exchanger reactor designs as well as other catalytic-wall reactor designs that are typically effected in microchemical systems. For $\delta > 0$, where the catalyst is internally cooled via the supporting wall/substrate, gains in effectiveness are observed for all values of the Thiele moduli when a substantial thermal gradient is imposed upon the catalyst layer (i.e., low thermal-conductivity and/or thick catalyst coatings are employed). Gains in selectivity are also observed for the series reaction as the position of the active zone at the fluid-side of the catalyst layer facilitates rapid removal of the desired product. However, increases in selectivity for the parallel reaction are solely dependent on the thermal favorability of ε_{pn}. For $\delta < 0$, where the catalyst is internally heated, increases in effectiveness are restricted by diffusion limitations while enhanced selectivities are observed to be thermally dependent for both series and parallel reactions. Thus, the presented analysis suggests that the use of thermally insulating and/or thick catalyst coatings capable of focusing thermal gradients within the catalytic region are favorable for internally

cooled conditions, especially for networks of consecutive reactions; this condition would correspond to exothermic reactions occurring in the presence of heat removal by the supporting wall, either as cooled reactors or as part of a heat-exchanger reactor design. Likewise, this analysis indicates that high conductivity and/or thin catalyst films are desirable for internally-heated conditions; this condition would correspond to endothermic reactions occurring in the presence of heat addition either by heat transfer fluid or as part of a heat-exchanger reactor configuration. Direct consideration of the interactions between the endothermic and exothermic layers will allow for validation of these observations.

III: MODELING OF COUPLED ENDOTHERMIC AND EXOTHERMIC CATALYST LAYERS

3.1. Model Derivation

As a more complete model, the coupled endothermic and exothermic catalyst layers were modeled simultaneously. This system allows for study of the intrinsic behavior of the heat exchanger reactor while isolating the system from reactor scale thermal effects. In order to model the system the coupled catalyst layers are folded such that equations may be developed subject to the same ordinate directions as illustrated in Figure 3.1.

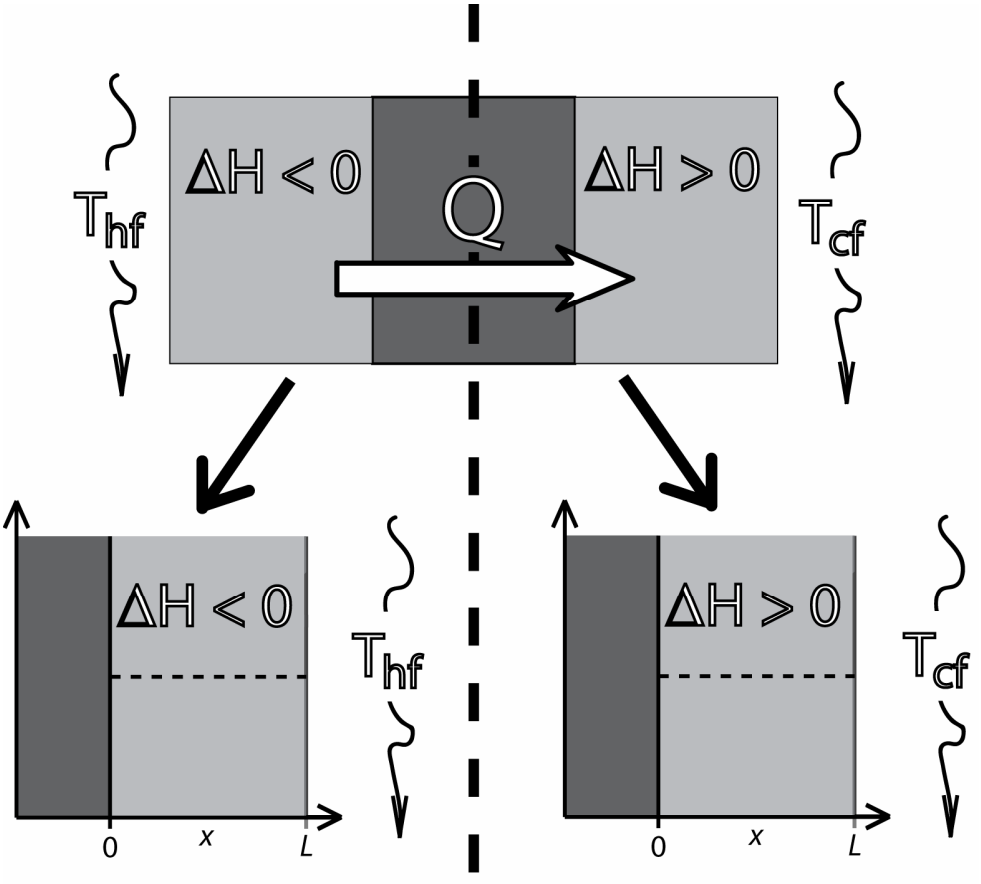

Figure 3.1: Illustration of the folding of the coupled system boundary conditions to allow for modeling of both layers subject to the same directional ordinates.

A single, irreversible reaction of the order *n* and *m* (exothermic and endothermic) is assumed for both catalyst layers. Further assuming that no convective mass transfer occurs within either layer, a mass balance for the exothermic side (variables denoted by a subscript *h*) yields equation 3.1:

$$\frac{\partial^2 c_h}{\partial x^2} = \frac{1}{D_{heff}} \cdot k_0 \exp\left[\frac{-E_h}{RT_h}\right] \cdot c_h^n \tag{3.1}$$

Which in dimensionless form is represented as:

$$\frac{\partial^2 u_h}{\partial s^2} = \phi_h^2 \cdot u_h^n \cdot \exp\left(\gamma_h \cdot \left\{\frac{v_h - 1}{v_h}\right\}\right) \tag{3.2a}$$

Where: $\phi_h^2 = \frac{L_h^2 c_{hf}^{n-1}}{D_{heff}} k_n\left(T_{hf}\right)$, $\gamma_h = \frac{E_h}{RT_{hf}}$, $s = \frac{x}{L}$, $u_h = \frac{c_h}{c_{hf}}$, and $v_h = \frac{T_h}{T_{hf}}$.

The equations for the endothermic side are analogous system and are denoted with a subscript *c*.

$$\frac{\partial^2 u_c}{\partial s^2} = \phi_c^2 \cdot u_c^n \exp\left(\gamma_c \cdot \left\{\frac{v_c - 1}{v_c}\right\}\right) \tag{3.2b}$$

In addition, *f* denotes the bulk fluid conditions.

By a similar method, an energy balance yields the equation for the temperature throughout the layer:

$$k_{hC} \frac{\partial^2 T_h}{\partial x^2} = \Delta H_{hR} \cdot k_0 \exp\left(\frac{-E}{RT_h}\right) \cdot c_h^n \tag{3.3}$$

$$\frac{d^2 v_h}{ds^2} = -\beta_h \cdot \phi_h^2 \cdot u_A^n \cdot \exp\left(\gamma_h \cdot \left\{\frac{v_h - 1}{v_h}\right\}\right) \tag{3.4a}$$

Where the Prater number is defined as: $\beta_h = \frac{-\Delta H_{hR} D_{eff} c_{hf}}{k_{hC} T_{hf}}$. Analogously, the equation for the endothermic side is:

$$\frac{d^2 v_c}{ds^2} = -\beta_c \phi_c^2 \cdot u_A^n \exp\left(\gamma_c \cdot \left\{\frac{v_c - 1}{v_c}\right\}\right) \tag{3.4b}$$

Boundary conditions are developed assuming fluid-solid diffusion limitations and a continuously stirred tank reactor mixing model at the fluid side and an impermeable wall of constant thermal conductivity. Therefore, *Robin* boundary conditions at the fluid side and no mass flux and equal heat flux conditions at the wall interface are applied.

At $s = 0$:

$$\frac{du_h}{ds} = 0 \quad \text{and} \quad \frac{dv_h}{ds} = \kappa_h\left(v_h - \chi v_c\right) \tag{3.5a}$$

$$\frac{du_c}{ds} = 0 \quad \text{and} \quad \frac{dv_c}{ds} = \kappa_c\left(v_c - \frac{v_h}{\chi}\right) \tag{3.5b}$$

At $s = 1$:

$$\frac{du_h}{ds} = Bi_{mh}\left(1 - u_h\right) \quad \text{and} \quad \frac{dv_h}{ds} = Bi_{hh}\left(1 - v_h\right) \tag{3.5c}$$

$$\frac{du_c}{ds} = Bi_{mc}\left(1 - u_c\right) \quad \text{and} \quad \frac{dv_c}{ds} = Bi_{hc}\left(1 - v_c\right) \tag{3.5d}$$

Where $\chi = \frac{T_{cf}}{T_{hf}}$ and $\kappa_h = \frac{k_w L_h}{k_{hC} L_w}$ while the Biot numbers are given as $Bi_{mh} = \frac{L \cdot k_{gh}}{D_{heff}}\left(\frac{\overline{V_h}}{\overline{V_h} + k_{gh} A}\right)$

and $Bi_{hh} = \frac{L_h \cdot h}{k_{hC}}\left(\frac{F_h C_p}{F_h C_p + hA}\right)$.

Effectiveness factors are also defined relative to bulk fluid conditions as in the Thiele paper. This maintains the effectiveness as the ratio of the reaction rate to the reaction rate in the absence of any transport limitations.

$$\eta_h = \frac{1}{\phi_h^2} \cdot \frac{du_h}{ds}\bigg|_0^1 \qquad \text{and} \qquad \eta_c = \frac{1}{\phi_c^2} \cdot \frac{du_c}{ds}\bigg|_0^1 \tag{3.6}$$

3.2. Procedure:

The dimensionless equations were solved in MatLab utilizing the user created boundary value solver *bvp6c* which is identical to the previously described *bvp4c* solver but in addition reports out the residual of the calculation in order to keep track of errors. The derivatives of the reacting species were used to determine effectiveness factors for both catalyst layers for several parameter values.

3.3 Results and Discussion

The effectiveness factors for the exothermic (h) and endothermic (c) layers are presented in Figure 3.3 for the representative case of $\beta_h = 0.25$, $\beta_c = -0.35$, $\gamma_h = \gamma_c = 20$, $\chi = 1$, and $\kappa_h = \kappa_c = 100$ as well as Biot numbers of 1000. The value of the Prater number for the endothermic catalyst is representative of the steam-reforming of methane [25, 26] while the value for the exothermic side represents the highest value of Prater number which the solver could determine solutions before. As mentioned previously, above particular values of the Prater number and activation energy (γ), the system is expected to have multiple solutions and as a result can not be solved for numerically. The value for κ reflects the ratio of the conductivity of steel to porous alumina [27, 28]. Figure 3.2 shows significant interactions between both catalyst layers as the diffusion limitations of one catalyst layer affect the effectiveness factor of the other.

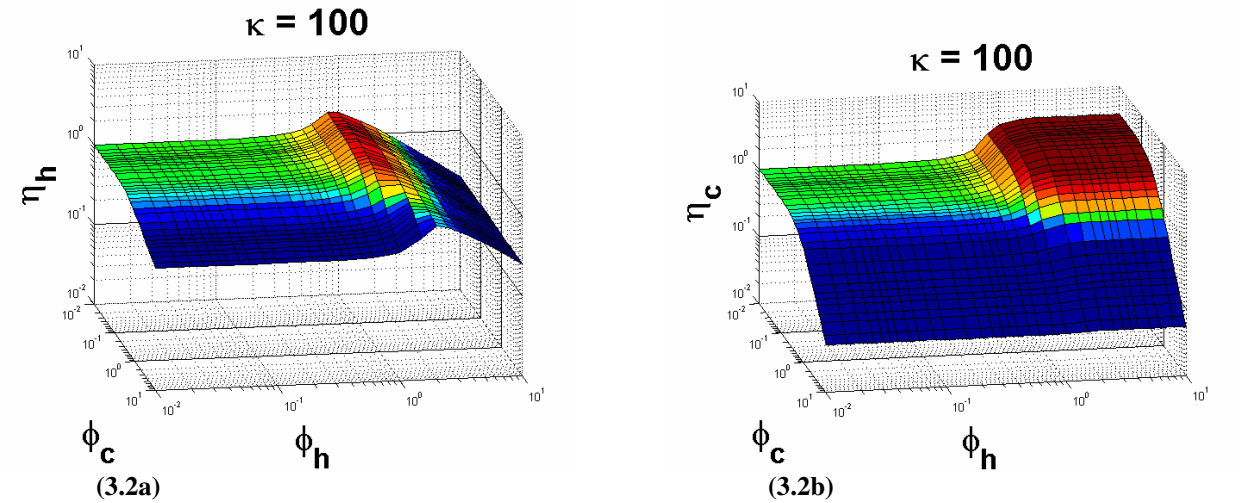

Figure 3.2: Values for the exothermic and endothermic catalyst layers for a steel support wall $\{\beta_h = 0.25, \beta_c = -0.35, \gamma_h = \gamma_c = 20, \chi = 1, \kappa_h = \kappa_c = 100, Bi_{mh} = Bi_{hh} = Bi_{mc} = Bi_{hc} = 1000\}$.

For the exothermic catalyst layer, increases effectiveness are observed for values of ϕ_h near one. Conversely, a decrease in hot-side effectiveness is observed with increasing values of ϕ_c. For the endothermic catalyst layer, increases in effectiveness are observed for all values of ϕ_h greater than one while the effectiveness decreases with increasing values of ϕ_c. Insight into the mechanism of these trends can be gained by examining the values of the dimensionless variables for concentration and temperature at the catalyst-wall interfaces as shown in Figure 3.3.

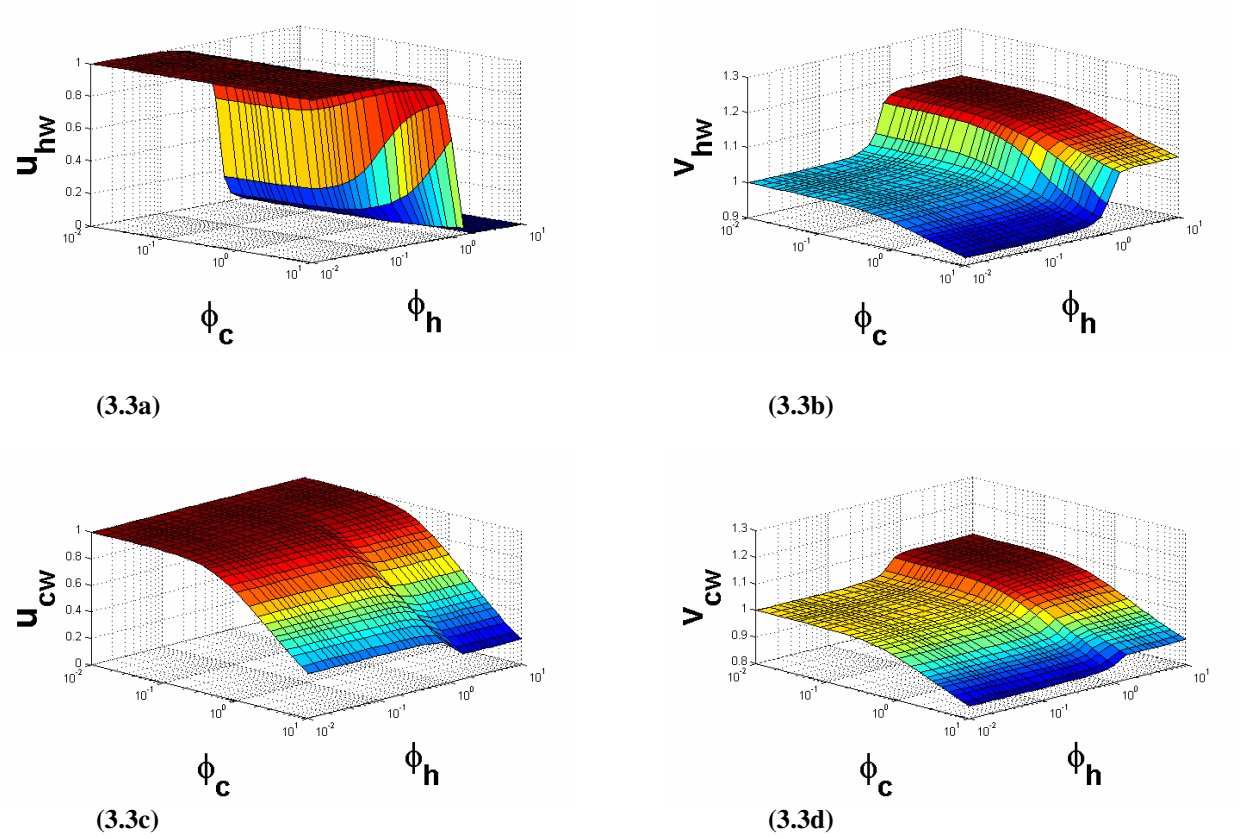

Figure 3.3: Dimensionless temperature and concentration at the catalyst wall-interfaces {β_h = 0.25, β_c = -0.35, $\gamma_h = \gamma_c$ = 20, χ = 1, $\kappa_h = \kappa_c$= 100, $Bi_{mh} = Bi_{hh} = Bi_{mc} = Bi_{hc}$ = 1000}.

On the hot catalyst (exothermic) side, u_{hw} decreases with increasing values of ϕ_h and therefore hot side diffusion limitations. Conversely, the values for v_{hw} increase. This indicates that, as more of the reactant is consumed before reaching the catalyst wall, an increase in the accumulation of heat occurs. Interestingly, for intermediate values of ϕ_h, u_{hw} increases with increasing values of ϕ_c. This can be explained by examining the values for u_{cw}, which decrease with increasing values of ϕ_c. This illustrates that an increasing amount of reactant is being consumed before reaching the wall as diffusion limitations increase. This results in the consumption of more heat by the endothermic reaction and a reduction in wall temperature which influences both catalyst layers, as shown in Figure 3.3. By a similar mechanism, the

dimensionless concentration of the endothermic reactant at the wall, u_{cw}, decreases and the temperature at the cold-side wall interface, v_{cw}, increases as the temperature at the wall of the hot-side, v_{hw}, increases.

Based on these observations, the effectiveness of the exothermic side increases for intermediate values of hot-side diffusion limitations as more of the reacting species is consumed before being fully distributed throughout the catalyst layer. Reaction heat then accumulates within the layer resulting in an increase in internal temperature and thereby reaction rate. For large values of ϕ_h, the consumption of the reactant results in a decrease in effectiveness despite increases in internal temperature. However, the effectiveness of the endothermic side is independent of the hot-side concentration and therefore does not decrease with high values of ϕ_h. The endothermic effectiveness decreases continuously with increasing cold-side diffusion limitations (ϕ_c) as both the reactant concentration and temperature decrease throughout the catalyst layer. Similarly, increases in ϕ_c also result in a decrease in exothermic side as effectiveness as the temperature of the catalysts on both sides of the wall is reduced.

While the previous case represented catalyst layers separated by a high thermal-conductivity steel wall, the system can also be investigated for conditions representative of a low thermal-conductivity ceramic (i.e. cordierite) support wall. Figures for $\kappa = 1$ and other parameters as before are presented below.

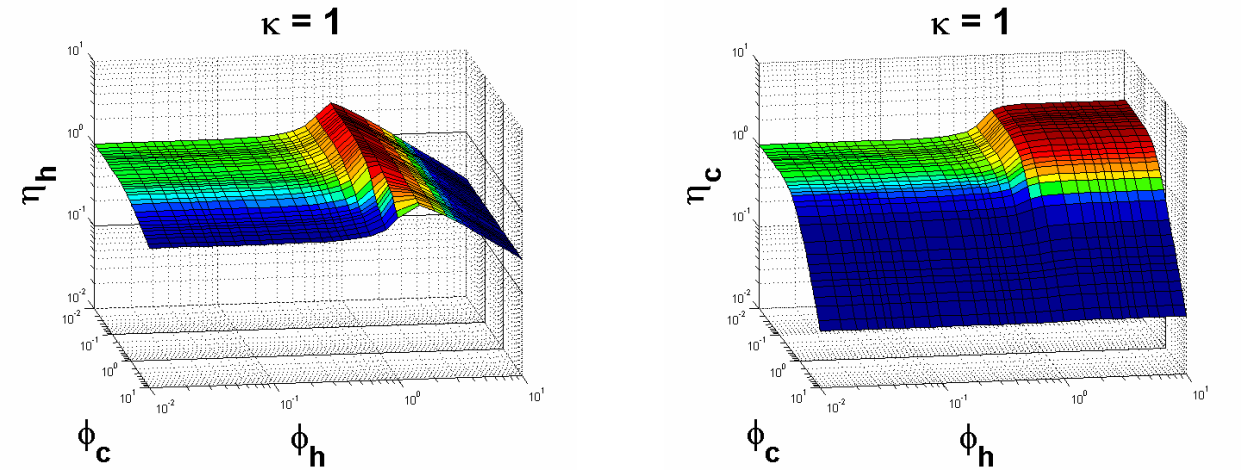

Figure 3.4: Exothermic and endothermic effectiveness factors for a ceramic support wall {β_h = 0.25, β_c = -0.35, $\gamma_h = \gamma_c$ = 20, χ = 1, $\kappa_h = \kappa_c$= 1, $Bi_{mh} = Bi_{hh} = Bi_{mc} = Bi_{hc}$ = 1000}.

Comparing these to Figure 3.2 shows that the effectiveness of the exothermic catalyst layer decreases slightly for the wall with higher conductivity (κ = 100), while the effectiveness of the endothermic catalyst layer increases. Therefore, more insulating supports allow for the accumulation of reaction heat in the exothermic catalyst layer while reducing the transport of the heat to the endothermic side.

The effect of alternate values of the Prater numbers for both reactions was also investigated. The results of the effectiveness for increasing values of β_h are presented in Figure 3.5 while the results for decreasing values of β_c are presented in Figure 3.6. Other parameter values match those previously reported for representing a ceramic support wall.

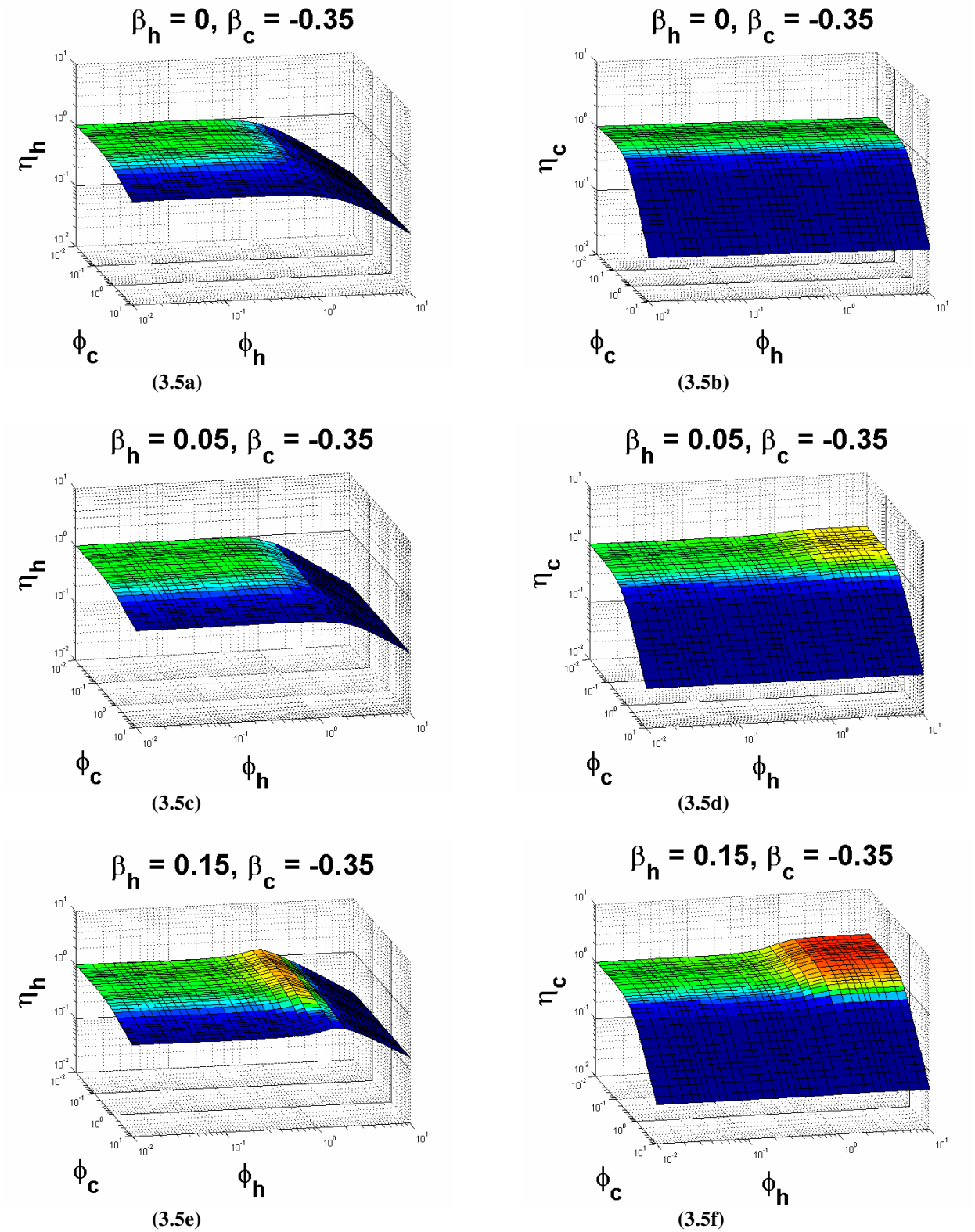

Figure 3.5: Effectiveness factors for increasing values of β_h $\{\gamma_h = \gamma_c = 20, \chi = 1, \kappa_h = \kappa_c = 1, Bi_{mh} = Bi_{hh} = Bi_{mc} = Bi_{hc} = 1000\}$.

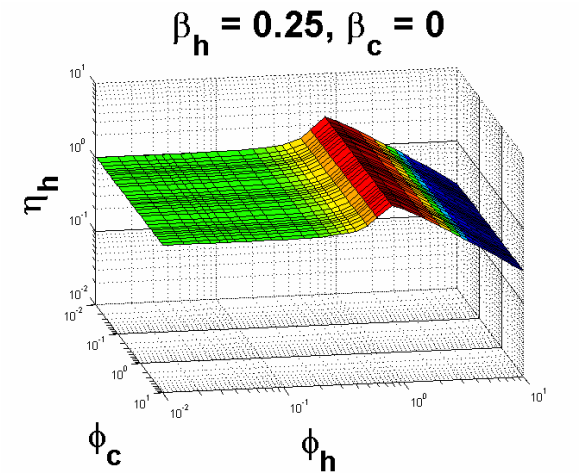

(3.6a)

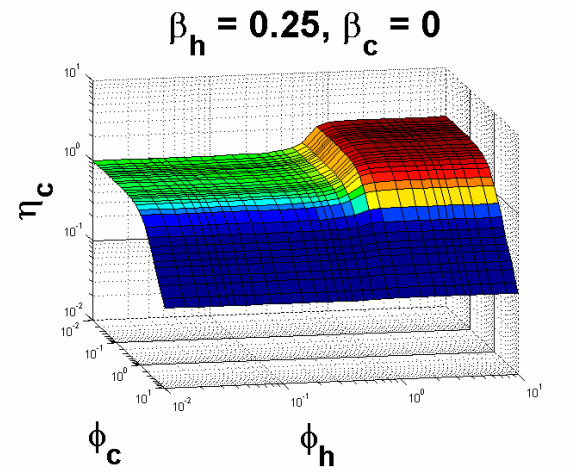

(3.6b)

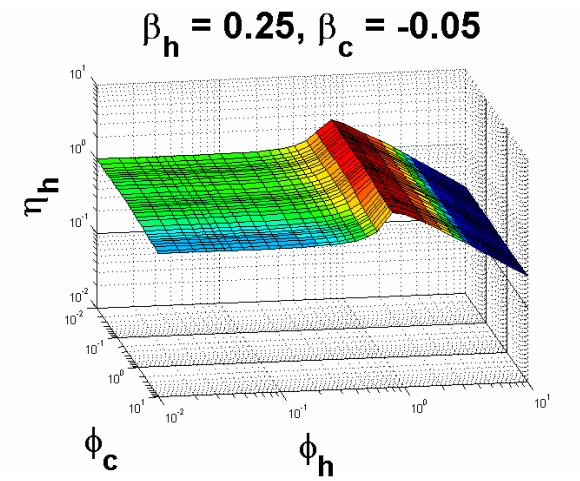

(3.6c)

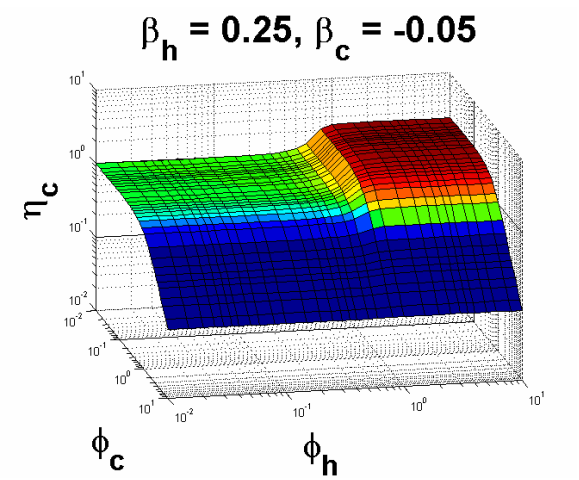

(3.6d)

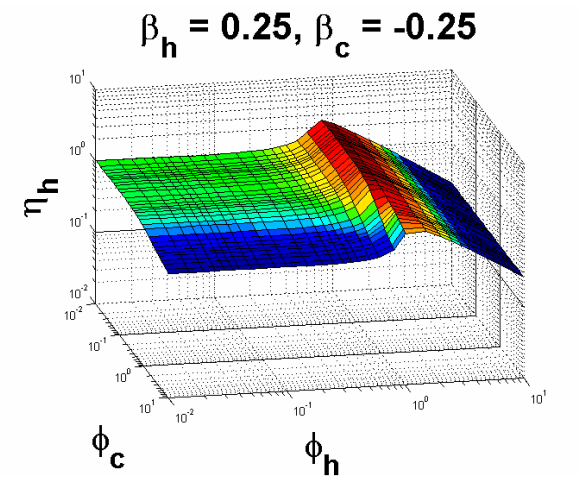

(3.6e)

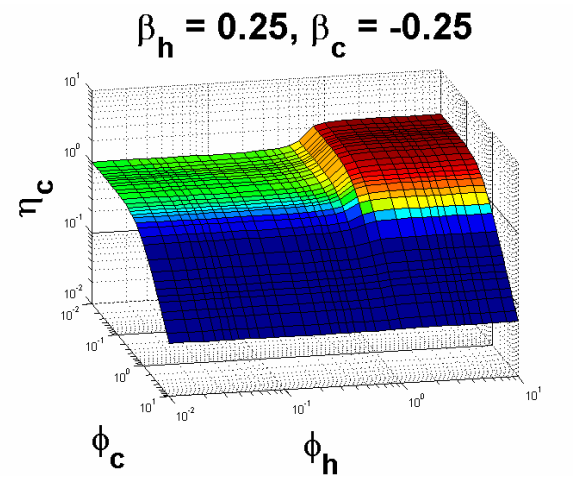

(3.6f)

Figure 3.6: Effectiveness factors for decreasing values of β_c { $\gamma_h = \gamma_c = 20$, $\chi = 1$, $\kappa_h = \kappa_c = 1$, $Bi_{mh} = Bi_{hh} = Bi_{mc} = Bi_{hc} = 1000$ }.

Higher values of exothermic reaction heats result in increases in the magnitude of peak effectiveness for both catalyst layers. More endothermic heats reaction on the cold-side results in a decrease in the effectiveness of the exothermic side for high values of ϕ_c. Any impact on the endothermic effectiveness is again less discernable as decreases in catalyst layer temperature coincide with decreases in reactant concentration.

3.4 Conclusions

There are significant, observable interactions between the coupled endothermic and exothermic catalyst layers. For intermediate values of ϕ_h, hot-side diffusion limitations result in the partial consumption of the reactant which in turn causes the accumulation of heat within the exothermic catalyst layer. The higher temperatures result in an increase in catalyst effectiveness for both catalyst layers. Conversely, high values of ϕ_c result in the consumption of heat and a drop in temperature of both catalyst layers which results in decreases in effectiveness. Using a support material with higher thermal conductivity results in increases in effectiveness for the endothermic side and decreases in effectiveness for the exothermic side. Also, higher values of the exothermic Prater number result in increases in effectiveness while more negative values of the endothermic Prater number result in decreases in effectiveness.

The primary conclusion to gain from this study is that intermediate values of ϕ_h (around 1) are desirable for increases in effectiveness on both the exothermic and endothermic side while low values of ϕ_c (at least 0.1) are required to maintain higher effectiveness factors on both sides. In a real device, assuming similar porosities and other properties between both catalyst layers, this suggests that the relative thickness of the catalyst layer on the exothermic side ought to be significantly greater (nearly ten times) the thickness of the endothermic catalyst layer.

Furthermore, these conclusions support those of the thermal gradient study in which thin catalyst films were found to be favorable for internally-heated (endothermic) conditions while thick catalyst coatings are more favorable for focusing of thermal gradients under internally-cooled (exothermic) conditions.

IV: FUTURE CONSIDERATIONS AND FINAL CONCLUSIONS

A significant consideration in the modeling of exothermic reactions which was not taken into full consideration in this study was the existence of multiplicity of solutions. Weisz and Hicks [6] acknowledged this possibility in their study of mass and heat diffusion effects in a spherical particle, however they did not mathematically develop sufficient conditions for stability. However, what they did observe was that for exothermic reactions where $\beta\gamma \geq 5$, there are a range of ϕ values for which multiple solutions exist. They also discussed how the curve for heat production may be non-linear and have an inflection point while heat removal is typically linear. The intersections between these curves represent steady states, still they did not analytically determine conditions where this occurs.

Luss [29] developed sufficient conditions for stability in a spherical particle by determining parameter values necessary for satisfying a change in sign of an integral equation which assumes a existence of a bifurcation point. Mathematically this is equivalent to:

$$\left(T - T_a\right)\frac{d\ln f(T)}{dT} \leq 1 \qquad \text{for all } T_a \leq T \leq T_{eq} \tag{4.1}$$

Where $f(T)$ is the reaction rate in terms of temperature and the subscripts represent *a* for ambient conditions and *eq* for equilibrium. For the first order, irreversible reaction, Eqn. 4.1 yields:

$$\beta\gamma \leq 4(1+\beta) \tag{4.2}$$

For the modeling of coupled endothermic and exothermic reactions, a maximum value of $\beta = 0.25$ for $\gamma = 20$ was investigated for the exothermic catalyst. Though for a different system, assuming similar behavior between geometries, the values used in the coupled system study fall within the criteria for uniqueness as given by Eqn. 4.2 (as $4 \leq 5$). More importantly than geometric differences, there is an additional heat removal term resulting from coupling the

exothermic layer with an endothermic layer. Therefore, it would be prudent to analytically establish conditions for uniqueness of the steady state when coupling exothermic and endothermic catalytic layers.

In addition to establishment of conditions for stability, it would also be worthwhile to define appropriate regions where multiplicity occurs, and, ideally, be capable of determining the effectiveness for all conditions. In order to accomplish this task, static and Hopf bifurcation methods would have to be applied to the time-variant partial differential equations of the system. This route was thoroughly developed by Jensen and Ray [30] to investigate the bifurcation behavior of the first order, irreversible reaction in a tubular reactor with axial dispersion. Though mathematically similar to the system they investigated, the inherent thermal coupling of our boundary conditions at the catalyst-wall interfaces left our system unamenable to any analogous treatment. Therefore, alternative methods for solution of the system would have to be determined.

Despite being unable to investigate the stability or multiplicity of the coupled system, significant and valuable insight into the inherent behavior of heat-exchanger microreactors was attained. Both the constant thermal gradient and coupled system studies found that the exothermic catalyst layer should be significantly thicker than the endothermic catalyst layer to maintain high values of effectiveness in both catalyst layers. This allows for accumulation of reaction heat within the system while allowing high rates of reaction in both exothermic and endothermic layers.

V: NOMENCLATURE

C_A	Molar concentration of species A, kmol.m^{-3}
C_{Af}	Bulk fluid molar concentration of species A, kmol.m^{-3}
C_p	Specific heat capacity of the bulk fluid, kJ.kg^{-1}.K^{-1}
D_{Aeff}	Effective diffusivity of species A, m^2.s^{-1}
$D_{A/B}$	Ratio of effective diffusivity of species A to species B
E_n	Activation energy of reaction n, kJ.kmol^{-1}
F_h	Mass flowrate of the bulk fluid in the exothermic channel, kg.s^{-1}
ΔH	Heat of reaction, kJ.kmol^{-1}
h	Heat transfer coefficient for bulk fluid in the exothermic channel, kJ.m^{-2}.K^{-1}.s^{-1}
k_{gh}	Mass transfer coefficient for bulk fluid in the exothermic channel, m.s^{-1}
k_{hC}	Thermal conductivity of the exothermic catalyst, kJ.m^{-1}.K^{-1}.s^{-1}
k_n	Rate coefficient for nth-order power-law reaction, m^{3j-3}.kmol^{j-1}.s^{-1}
k_{nf}	Rate coefficient for reaction n at the bulk-fluid temperature, m^{3j-3}.kmol^{j-1}.s^{-1}
L	Catalyst film thickness, m
R	Universal gas constant, kJ.kmol^{-1}.K^{-1}
s	Dimensionless position within the catalyst
T	Temperature within catalyst at position x, Kelvin
T_f	Bulk fluid temperature, Kelvin
T_w	Wall temperature, Kelvin
u_A	Dimensionless concentration of species A
$\overline{V}_h$	Volumetric flowrate of the bulk fluid in the exothermic channel, m^3.s^{-1}
v	Dimensionless temperature

x	position within catalyst, m

Greek Letters:

β_h	Prater number for the exothermic reaction
δ	Dimensionless thermal gradient magnitude
ε_{mn}	Ratio of activation energy of reaction m to reaction n
γ_n	Dimensionless activation energy of reaction n
κ_h	Dimensionless ratio of wall to catalyst thermal conductivities (coupled system)
κ_{mnf}	Dimensionless ratio of reaction rates (thermal gradient system)
η	Catalyst effectiveness, Eq. 4
ϕ	Thiele modulus

VI: REFERENCES

[1] L. D. Schmidt. *The Engineering of Chemical Reactions*. Oxford University Press, New York 2005.

[2] E.W. Thiele. Relation between catalytic activity and size of particle. *Ind. Eng. Chem.* 31 (1939) 916-920.

[3] R. Aris. On Shape Factors for Irregular Particles – I. The Steady-State Problem. Diffusion and Reaction. *Chem. Eng. Sci.* 6 (1957) 3899-3903.

[4] E.R. Becker and J. Wei. Nonuniform distribution of catalysts on supports: I. Bimolecular Langmuir reactions. *J. Catal.* 46 (1977) 365-371.

[5] C.J. Pereira and A. Varma. Uniqueness criteria of the steady state in automotive catalysts. *Chem. Eng. Sci.* 33 (1978) 1645-1657.

[6] P.B. Weisz and J.S. Hicks. The behaviour of porous catalyst particles in view of internal mass and heat diffusion effects. *Chem. Eng. Sci.* 17 (1962) 265-275.

[7] I. Copelowitz and R. Aris. Communications on the theory of diffusion and reaction – VI. The effectiveness of spherical catalyst particles in steep external gradients. *Chem. Eng. Sci.* 25 (1970) 885-896.

[8] X. Ouyang, L. Bednarova, R.S. Besser and P. Ho. Preferential oxidation in a thin-film catalytic microreactor: Advantages and Limitations. *AIChE J.* 51 (2005) 1758-1772.

[9] P. Reuse, A. Renken, K. Haas-Santo, O. Görke and K. Schubert. Hydrogen production for fuel cell application in an autothermal micro-channel reactor. *Chem. Eng. J.* 101 (2004) 133-141.

[10] E.R. Delsman, M.H.J.M. de Croon, G.J. Kramer, P.D. Cobden, Ch. Hofmann, V. Cominos and J.C. Schouten. Experiments and modeling of an integrated preferential oxidation-heat exchanger microdevice. *Chem. Eng. J.* 101 (2004) 123-131.

[11] B.A. Wilhite, S.E. Weiss, J.Y. Ying, M.A. Schmidt and K.F. Jensen. High-Purity Hydrogen Generation in a Microfabricated 23 wt % Ag-Pd Membrane Device Integrated with 8:1 $LaNi_{0.95}Co_{0.05}O_3/Al_2O_3$ Catalyst. *Adv. Mater.* 18 (2006) 1701-1704.

[12] A. Basile, A. Criscuoli, F. Santella and E. Drioli. Membrane reactor of water gas shift reaction. *Gas. Sep. Purif.* 10 (1996) 243-254.

[13] G. Kolios, B. Glöckler, A. Gritsch, A. Morillo and G. Eigenberger. Heat-integrated reactor concepts for hydrogen production by methane steam reforming. *Fuel Cells* 5 (2005) 52-65.

[14] G. Kolb, J. Schürer, D. Tiemann, M. Wichert, R. Zapf, V. Hessel and H. Löwe. Fuel processing in integrated micro-structured heat-exchanger reactors. *J. Power Sources* 171 (2007) 198-204.

[15] J.D. Holladay, Y. Wang, E. Jones. Review of developments in portable hydrogen production using microreactor technology. *Chem. Rev.* 104 (2004) 4767-4790.

[16] K.F. Jensen. Microreaction engineering – is small better? *Chem. Eng. Sci.* 56 (2001) 293-303.

[17] M. Lee, R. Greif, C.P. Grigoropoulos, H. G. Park, F. K. Hsu. Transport in packed-bed and wall-coated steam- methanol reformers. *J. Power Sources* 166 (2007) 194-201.

[18] A. Karim, J. Bravo, D. Gorm, T. Conant and A. Datye. Comparison of wall-coated and packed-bed reactors for steam reforming of methanol. *Catal. Today* 110 (2005) 86-91.

[19] S.R. Deshmukh and D.G. Vlachos. Effect of flow configuration on the operation of coupled combustor/reformer microdevices for hydrogen production. *Chem. Eng. Sci.* 60 (2005) 5718-5728.

[20] R.C. Ramaswamy, P.A. Ramachandran and M.P. Dudukovic. Recuperative coupling of exothermic and endothermic reactions. *Chem. Eng. Sci.* 61 (2006) 459-472.

[21] A. Moreno, K. Murphy and B.A. Wilhite. Parametric Study of Solid-Phase Axial Heat Conduction in Thermally Integrated Microchannel Networks. *Ind. Eng. Chem. Res.* 47 (2008) 9040-9054.

[22] G. Arzamendi, P.M. Diéguez, M. Montes, M.A. Centeno, J.A. Odriozola and L. M. Gandía. Integration of methanol steam reforming and combustion in microchannel reactor for H_2 production: A CFD simulation study. *Catal. Today* 143 (2009) 25-31.

[23] H. Mei, C. Li, S. Ji and H. Liu. Modeling of a metal monolith catalytic reactor for methane steam reforming – combustion coupling. *Chem. Eng. Sci.* 62 (2007) 4294-4303.

[24] R. Aris. *The Mathematical Theory of Diffusion and Reaction in Permeable Catalysts*. Oxford University Press, New York 1975.

[25] R.E. Hayes, S.T. Kolaczkowskib, P.K.C. Li, and S. Awdry. Evaluating the effective diffusivity of methane in the washcoat of a honeycomb monolith. *Applied Catalysis B: Environmental* 25 (2000) 93-104.

[26] K. Hou and R. Hughes. The kinetics of methane steam reforming over a Ni/α-Al_2O catalyst. *Chem. Eng. J.* 82 (2001) 311-328.

[27] R.A. Mischke and J.M. Smith. Thermal conductivity of alumina catalyst pellets. *Ind. Eng. Chem. Fundamen.* 1 (1962) 288-292.

[28] R.H. Perry and D.W. Green ed. *Perry's Chemical Engineers' Handbook, 8th Edition.* McGraw-Hill, New York (2007).

[29] D. Luss. Sufficient conditions for uniqueness of the steady state solutions in distributed parameter systems. *Chem. Eng. Sci.* 23 (1968) 1249-1255.

[30] K.F. Jensen and W.H. Ray. The bifurcation behavior of tubular reactors. *Chem. Eng. Sci.* 37 (1982) 199-222.